Enhanced Capacitance of Composite Anodic ZrO_2 Films Comprising High Permittivity Oxide Nanocrystals and Highly Resistive Amorphous Oxide Matrix

Hiroki Habazaki,[†,*] *Shun Koyama,*[†] *Yoshitaka Aoki,*[†] *Norihito Sakaguchi,*[‡] *Shinji Nagata*[§]

[†] Division of Materials Chemistry, Faculty of Engineering, Hokkaido University, Sapporo, Hokkaido, 060-8628, Japan

[‡] Center for Advanced Research of Energy and Materials, Faculty of Engineering, Hokkaido University, Sapporo, Hokkaido, 060-8628, Japan

[§] Institute for Materials Research, Tohoku University, 2-1-1 Katahira, Sendai 980-8577, Japan

Corresponding author, Phone & Fax: +81-11-706-6575, e-mail: habazaki@eng.hokudai.ac.jp

RECEIVED DATE

Anodic oxide films with nanocrystalline tetragonal ZrO_2 precipitated in an amorphous oxide matrix were formed on Zr-Si and Zr-Al alloys and had significantly enhanced capacitance in comparison with those formed on zirconium metal. The capacitance enhancement was associated with the formation of a high-temperature stable tetragonal ZrO_2 phase with high relative permittivity as well as increased ionic resistivity, which reduces the thickness of anodic oxide films at a certain formation voltage. However,

there is a general empirical trend that single-phase materials with higher permittivity have lower ionic resistivity. This study presents a novel material design based on a nanocrystalline-amorphous composite anodic oxide film for capacitor applications.

KEYWORDS: Anodic oxide, Dielectric film, Nanocomposite oxide, ZrO_2, Capacitor

1. INTRODUCTION

Miniaturization of high-performance electrical devices and components is a contemporary need in the microelectronics industry for the design of portable electronic devices, including computers and telecommunications devices. Solid electrolytic tantalum capacitors play a major role in the passive component industry due to their high reliability, high capacitance, low leakage current, and low equivalent series resistance.[1, 2] Because there is still a constant demand to improve the volume efficiency, many efforts have been made to enhance the capacitance of various capacitors, gate dielectrics, and so on.[3-5]

The capacitance of capacitors is given by the following equation:

$$C = \varepsilon_0 \varepsilon_{ox} S/d \qquad (1)$$

where ε_0 is the permittivity of vacuum, ε_{ox} is the relative permittivity of dielectric oxide, S is the surface area, and d is the thickness of the dielectric oxide film. Thus, in addition to increasing the surface area, which is the main approach that has been considered by the current tantalum capacitor industry, the volume efficiency can be increased by increasing the relative permittivity and decreasing the thickness of dielectric films. In electrolytic capacitors, dielectric films are formed by anodizing metals, which act as anodes in the capacitor. The thickness of the dielectric films is controlled according to the following equation:

$$d = \alpha V_f \qquad (2)$$

where V_f is the formation voltage and the proportional constant α is the formation ratio. Because V_f must be larger than the operating voltage of capacitors to ensure reliability, the key parameters that

control the capacitance are α and ε_{ox}. Enhancing the ε_{ox} value and lowering the α value enhance capacitance. However, there is a positive empirical correlation between ε_{ox} and α (Figure 1).[6] Thus, even if anodic Ta_2O_5 (ε_{ox} = 27) is replaced with anodic Nb_2O_5 (ε_{ox} = 42), the capacitance is not highly enhanced due to the formation of a thicker anodic oxide film in the case of Nb_2O_5.

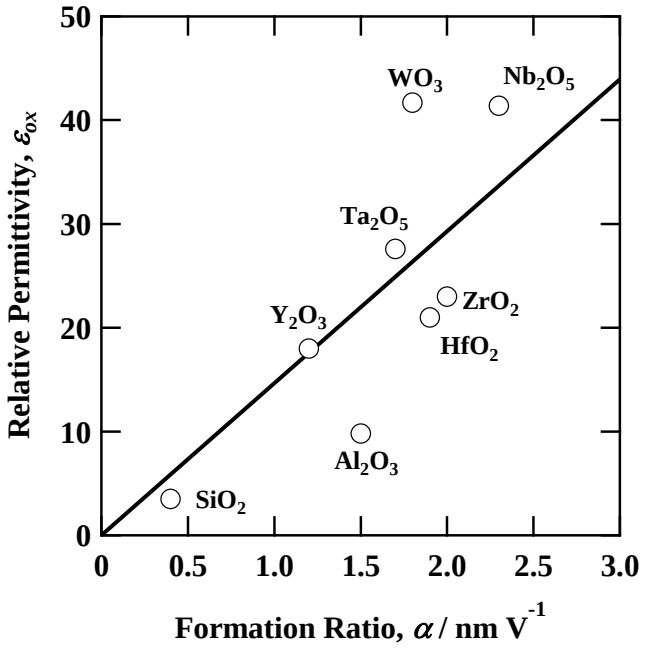

Figure 1. Correlation between relative permittivity and formation ratio of various anodic oxides formed on valve metals.

Valve metals such as aluminum,[7-13] niobium,[14-18] and titanium[19-25] were alloyed in order to control the properties of anodic oxide films and improve their dielectric properties. The general trend in amorphous anodic oxide films is that their properties on binary valve metal alloys—including the relative permittivity and formation ratio—are the compositional averages of the respective alloy-constituting metals. An example of the relative permittivity of anodic oxide films on Al-Ta and Nb-Ta binary alloys is shown in Fig. 2. All the anodic oxides on these alloys are amorphous. As seen in this figure, the permittivity changes linearly with the alloy composition. Similar trends have also been observed for the

formation ratio.

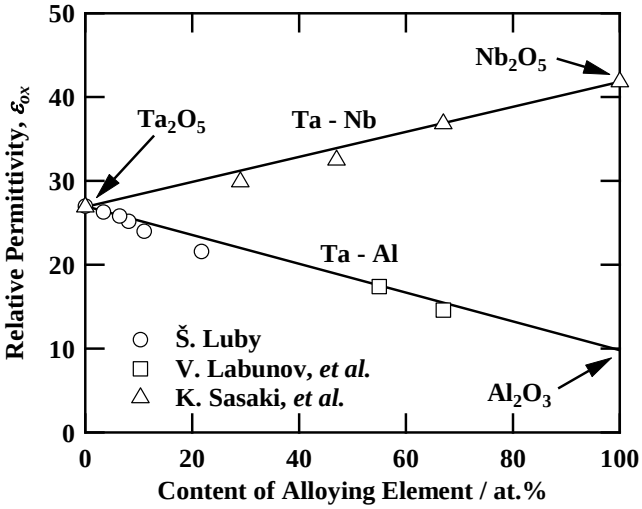

Figure 2. Compositional dependence of relative permittivity of anodic oxides formed on Ta–Al and Ta–Nb alloys.[26-28]

Here, we report the marked enhancement in the capacitance of anodic oxides on binary alloys by the formation of ZrO_2-based composite oxide films with nanocrystalline oxide precipitates in an amorphous matrix. Alloying zirconium with a suitable amount of silicon or aluminum leads to an increase in the permittivity of the oxide and a decrease in the formation ratio, which results in the marked capacitance enhancement. The increase in permittivity was attributed to the formation of the tetragonal ZrO_2 phase that has higher permittivity than thermodynamically stable monoclinic ZrO_2, which is the major phase in the anodic oxide on zirconium. The decrease in the formation ratio was associated with the enrichment of silicon and aluminum in the amorphous oxide matrix because anodic Al_2O_3 and SiO_2 have higher ionic resistivity than anodic ZrO_2. The findings of this study open up a new paradigm in design of high dielectric materials for capacitor applications.

2. EXPERIMENTAL DETAILS

Thin films of zirconium, Zr-3.6 at% Y, Zr-10 at% Si, and Zr-11 at% Al were prepared by magnetron sputtering on flat glass and aluminum substrates. These alloy compositions were selected because the highest capacitance was obtained in each alloy system. Prior to sputtering, the latter substrate was electropolished and subsequently anodized to 200 V in 0.1 mol dm^{-3} ammonium pentaborate electrolyte to provide a flat surface. The specimens prepared on the aluminum substrate were mostly used for characterizing the anodic oxide films by transmission electron microscopy (TEM) and Rutherford backscattering spectroscopy (RBS). The targets used for preparation of the alloy films were a 99.9% zirconium disk 100 mm in diameter with selected numbers of 99.5% yttrium chips, 99.999% silicon plates, or 99.99% aluminum plates located symmetrically on the erosion region. The zirconium disk without alloying element chips or plates was used for preparation of the zirconium films. Alloy compositions were determined by Rutherford backscattering spectroscopy (RBS) or electron probe microanalysis (JEOL JXA-8900M).

The specimens were anodized at several formation voltages up to 100 V for 900 s in stirred 0.1 mol dm^{-3} ammonium pentaborate electrolyte at 298 K using a two-electrode cell with a platinum counter electrode. Initially, a constant current density of 50 A m^{-2} was applied to reach the selected formation voltage. Electrochemical impedance measurements were carried out in the same electrolyte by applying a 50 mV (rms) sinusoidal alternating voltage in the 10^0–10^4 Hz range, and the capacitances of the anodic oxide films were determined by analyzing the Bode diagrams.

Vertical cross-sections of the anodic oxide films were observed using a TEM (JEOL JEM-2000FX or Hitachi HD-2000) operating at 200 kV. High-resolution transmission electron microscopy (HRTEM) of the films was carried out using a FEG-TEM (JEOL JEM-2010F) operating at 200 kV. Electron transparent sections approximately 30-nm thick were generated using an ultramicrotome (Reichert-Nissei Ultracut S) with a diamond knife. The structures of the deposited films and anodic oxide films were identified by grazing incidence X-ray diffraction (GIXRD) using Cu Kα radiation with the

incident angle of 2° (Rigaku, RINT-2000 system). Raman measurements of anodic oxide films were performed using a 531.9-nm laser with a Synapse CCD detector. Laser power at the sample surface was maintained at 6 mW. Compositions of anodic oxide films and alloy films were determined by RBS using a 2.0 MeV He^{2+} ion beam supplied by a tandem-type accelerator at Tohoku University. The scattered particles were detected at 170° to the incident beam direction, which was normal to the specimen surface. The data were analyzed using the RUMP program. Furthermore, an elemental depth profile analysis was conducted by glow discharge optical emission spectroscopy (GDOES) using a Jobin-Ybon 5000 instrument in argon atmosphere of 600 Pa and applying a RF wave of frequency 13.56 MHz and power 35 W. Light emissions of characteristic wavelengths were monitored throughout the analysis with a sampling time of 0.01 s to obtain depth profiles. The signals were detected from a circular area of approximately 4 mm diameter.

3. RESULTS AND DISCUSSION

Figure 3 shows the change in the reciprocal of the capacitance for the anodic oxide films on zirconium, Zr-3.6 at% Y, Zr-10 at% Si, and Zr-11 at% Al films with the formation voltage. Because the thickness of the anodic oxide films is proportional to the formation voltage, there is a linear correlation between the reciprocal of the capacitance and the formation voltage for zirconium and its alloys containing yttrium and aluminum in accordance with Eq. (1). In contrast, a deviation from the linear correlation was found for Zr-10 at% Si; this was associated with a progressive amorphous-to-crystalline transition of anodic oxide with the formation voltage.[29, 30] The addition of yttrium to zirconium only slightly enhanced the capacitance, while the capacitance was markedly enhanced by the addition of silicon and aluminum. The capacitances of the anodic oxide films on Zr-10 at% Si and Zr-11 at% Al were 1.7 and 1.9 times that on zirconium at the formation voltage of 100 V. Such marked capacitance enhancement did not occur in the case of the Zr-Y alloys even if the yttrium content was increased up to 7.4 at% (See Figure S1 in Supporting Information).

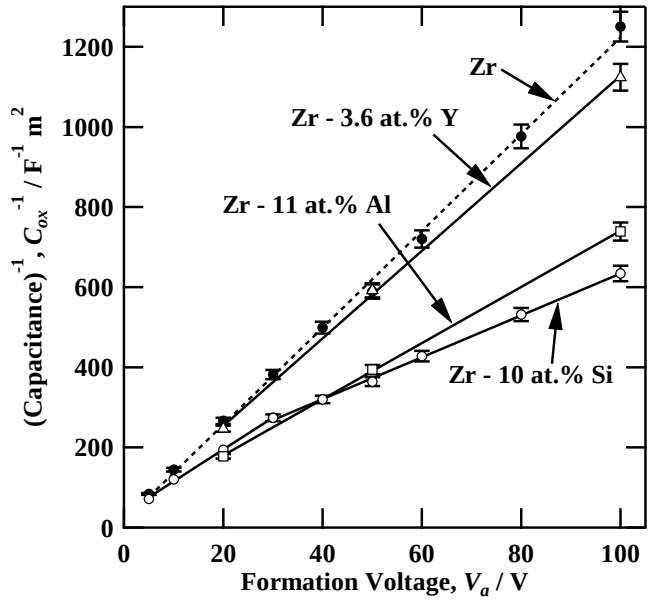

Figure 3. Change in reciprocal of capacitance of anodic oxide films, formed on sputter-deposited zirconium, Zr-3.6 at% Y, Zr-10 at% Si, and Zr-11 at% Al alloys in 0.1 mol dm^{-3} ammonium pentaborate electrolyte at 298 K for 900 s, with formation voltage.

Figure 4 shows the comparison of the capacitance, relative permittivity, and film thickness of the anodic oxide films formed on the zirconium and three zirconium alloys at 100 V. All alloying elements, i.e., yttrium, silicon, and aluminum, clearly enhanced the relative permittivity of anodic oxide, while the film thickness was largely dependent upon the alloying element. The addition of yttrium thickened the film from 270 nm to 317 nm. In contrast, the addition of silicon resulted in a marked decrease in the film thickness to 155 nm. Film thinning also occurred when aluminum was added to zirconium. The enhanced permittivity caused by the addition of yttrium was compensated for by film thickening, so the capacitance enhancement in the anodic oxide films on Zr-Y alloys was very limited. Both permittivity enhancement and film thinning were achieved by the addition of silicon and aluminum, leading to a marked enhancement in capacitance. Fig. 1 shows that the formation ratio of ZrO_2 is likely reduced by the addition of Y_2O_3, SiO_2, and Al_2O_3 and that a decrease in the relative permittivity can be predicted

upon the addition of these oxides. Thus, unexpected capacitance enhancement was realized by the addition of SiO_2 and Al_2O_3 to anodic ZrO_2. Note that the leakage current does not increase even if the capacitance increases.[30]

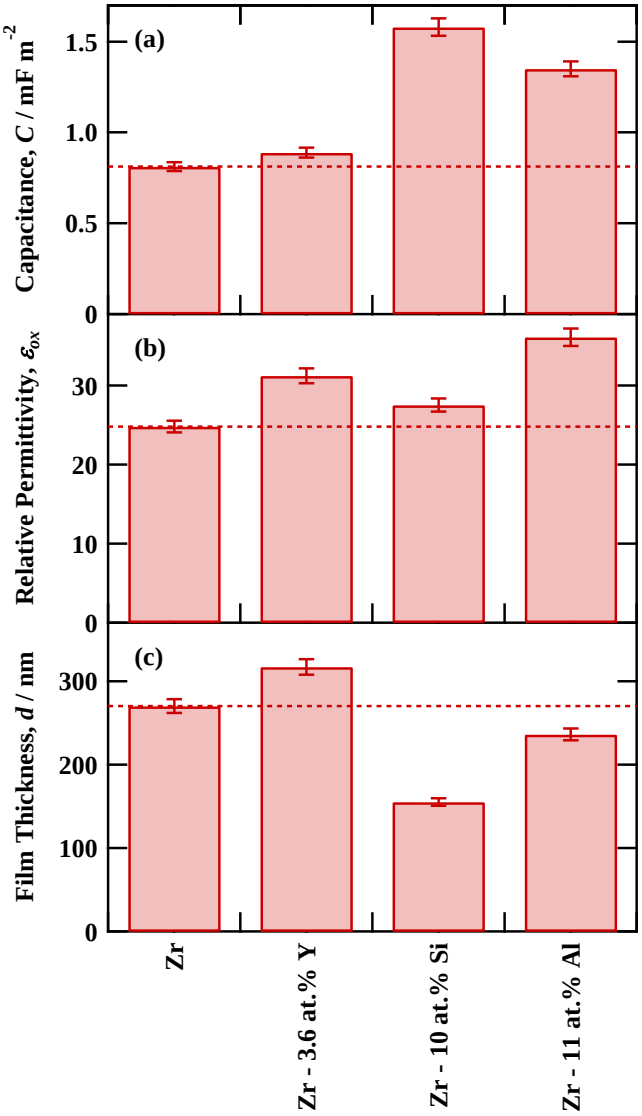

Figure 4. (a) Capacitance, (b) relative permittivity, and (c) film thickness of the anodic oxide films formed on zirconium, Zr–3.6 at% Y, Zr–10 at% Si, and Zr–11 at% Al alloys at 100 V in 0.1 mol dm^{-3} ammonium pentaborate electrolyte at 298 K for 900 s.

To clarify the role of individual alloying elements in the film thickness and permittivity of anodic

oxide films, the films were characterized by XRD, TEM, Raman spectroscopy, and glow discharge optical emission spectroscopy (GDOES) elemental depth profile analysis. Zirconium and hafnium, are known to usually form crystalline anodic oxides, although anodic oxides formed on many metals including aluminum, bismuth, niobium, silicon, tantalum, and tungsten are amorphous.[31] The anodic oxide film formed on zirconium in this study was also crystalline and mainly comprised monoclinic ZrO_2 (Figure 5), which is the thermodynamically stable phase at ambient temperature. In contrast, high-temperature stable tetragonal ZrO_2 was predominant in the anodic oxide films on all of the alloys containing yttrium, silicon and aluminum. The relative permittivity of doped tetragonal ZrO_2 is known to be larger than that of monoclinic ZrO_2.[32-34] The ε_{ox} values of the anodic oxide films formed on the Zr–Y and Zr–Al alloys agreed with the previously reported tetragonal ZrO_2. Thus, the enhanced permittivity due to alloying with yttrium and aluminum should be mainly associated with the formation of tetragonal ZrO_2. The slight enhancement in the permittivity by the alloying of zirconium with silicon may also be associated with the phase transformation to the tetragonal phase, but the presence of an amorphous phase in the anodic oxide film, as discussed later, may diminish the enhancement.

The high-temperature stable tetragonal ZrO_2 phase can be present even at ambient temperature through yttrium doping. The tetragonal ZrO_2 phase is also stabilized by the addition of silicon[35, 36] and aluminum,[37, 38] although the solubility of SiO_2 and Al_2O_3 to ZrO_2 is limited to 1 at% or less at equilibrium.[39, 40] Thus, it is reasonable that the tetragonal ZrO_2 phase is formed in the anodic ZrO_2 films that incorporate with yttrium, silicon and aluminum species. The formation of the tetragonal phase was also confirmed by Raman spectroscopy (Figure S2 in Supporting Information).

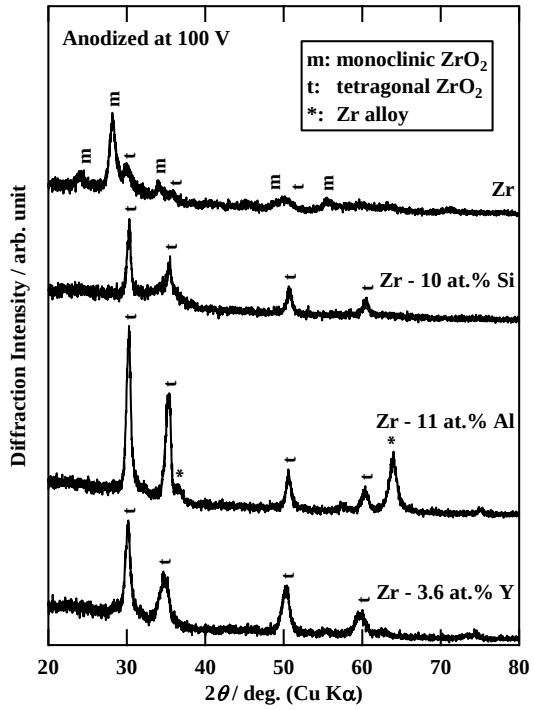

Figure 5. GIXRD patterns of the sputter-deposited zirconium, Zr–3.6 at% Y, Zr–10 at% Si, and Zr–11 at% Al alloys, after anodizing at 100 V in 0.1 mol dm^{-3} ammonium pentaborate electrolyte at 298K for 900 s.

The structure and thickness of the anodic oxide films were also examined by TEM observations (Figure 6). A 270 nm thick anodic oxide film with flat and parallel metal/film and film electrolyte interfaces was developed on zirconium, which appears at the bottom of the micrograph in Fig. 6a. The anodic oxide film consisted of nanocrystalline grains of 10–20 nm. A similar anodic oxide film consisting of nanocrystalline grains throughout the film thickness was formed on the yttrium-containing alloy, but the anodic oxide film was thicker than that on zirconium (Fig. 6b). The highly reduced film thicknesses of the anodic oxide films on the Zr–Si and Zr–Al alloys are visible in Figs. 6c and d. The anodic oxide films on the Zr–Si and Zr–Al alloys were apparently two layers. For Zr–10 at% Si, an inner layer that was 29% of the film thickness was amorphous, while an outer layer was amorphous on the Zr–11 at% Al. The anodic oxide films formed on the Zr–10 at% Si up to 30 V were amorphous

throughout the film thickness.[30] With further anodizing to higher voltages, crystallization of the outer layer proceeded with the relative thickness of the outer layer increasing with the formation voltage.[26, 27] The crystallization of the outer layer was associated with the formation of a thin outer ZrO_2 layer free from silicon species.[29, 30] Due to such progressive amorphous-to-crystalline transition, no linear correlation between the reciprocal of the capacitance and the formation voltage was obtained for the anodic oxide films on Zr–10 at% Si (Fig. 3).

When aluminum was added to zirconium, the anodic oxide films contained aluminum species throughout the film thickness, and crystalline oxide was formed even at low formation voltages. The formation of an amorphous layer in the outer part of the film should be related to the incorporation of boron species derived from the electrolyte.[41] Yttrium species were also distributed throughout the film thickness; this was confirmed by GDOES depth profile analysis (Figure S3 in Supporting Information).

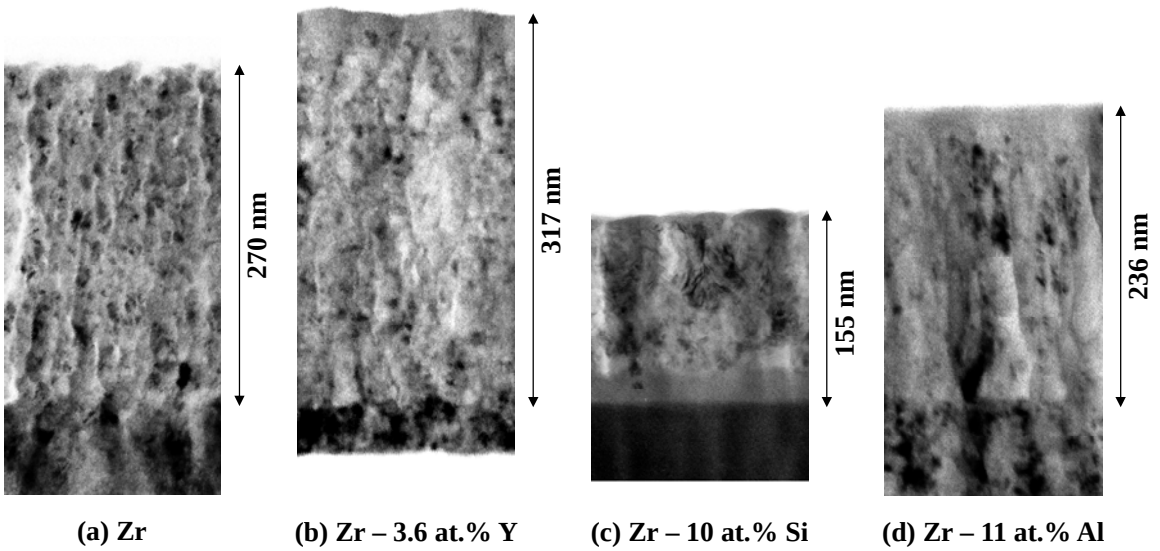

Figure 6. Transmission electron micrographs of ultramicrotomed vertical cross sections of the sputter-deposited (a) zirconium, (b) Zr–3.6 at% Y, (c) Zr–10 at% Si, and (d) Zr–11 at% Al alloys, after anodizing at 100 V in 0.1 mol dm^{-3} ammonium pentaborate electrolyte at 298 K for 900 s.

The addition of trivalent yttrium species to ZrO_2 introduces oxygen vacancies in crystalline lattice of ZrO_2. Since migration of oxide ions occurs predominantly during the growth of the crystalline anodic ZrO_2, the introduction of oxygen vacancies reduces the ionic resistivity of anodic ZrO_2 and increases the film thickness in anodizing at a certain constant voltage. The thinning of the anodic oxide films by the addition of silicon and aluminum is related to the formation of a composite oxide layer comprised nanocrystalline tetragonal ZrO_2 and an amorphous matrix, as seen in the high-resolution transmission electron micrographs (Figure 7). The spacing of the lattice fringes found in the micrographs was 0.30 nm, which corresponds to the spacing of (101) plane of tetragonal ZrO_2. The micrographs reveal the presence of amorphous regions in addition to the crystalline ZrO_2 phase in the crystalline layers of the anodic oxide films on the Zr–10 at% Si and Zr–11 at% Al alloys. The limited solubility of SiO_2 and Al_2O_3 to ZrO_2 should induce the phase separation into tetragonal ZrO_2 and an amorphous matrix. The crystalline ZrO_2 must contain a limited amount of silicon or aluminum ions, so the amorphous matrix should be enriched in silicon or aluminum. Anodic SiO_2 and Al_2O_3 have a markedly reduced formation ratio compared with anodic ZrO_2 (Fig. 1). The silicon- or aluminum-enriched amorphous matrix may contribute mainly to the thinning of the anodic oxide films on the Zr–Si and Zr–Al alloys. The field strengths in the growing inner amorphous and outer crystalline layers on Zr–10 at% Si (Fig. 6c) were estimated to be 0.45 and 0.70 GV m^{-1}, respectively. The greatly increased field strength of the crystalline layer may result from the formation of the silicon-enriched amorphous matrix.

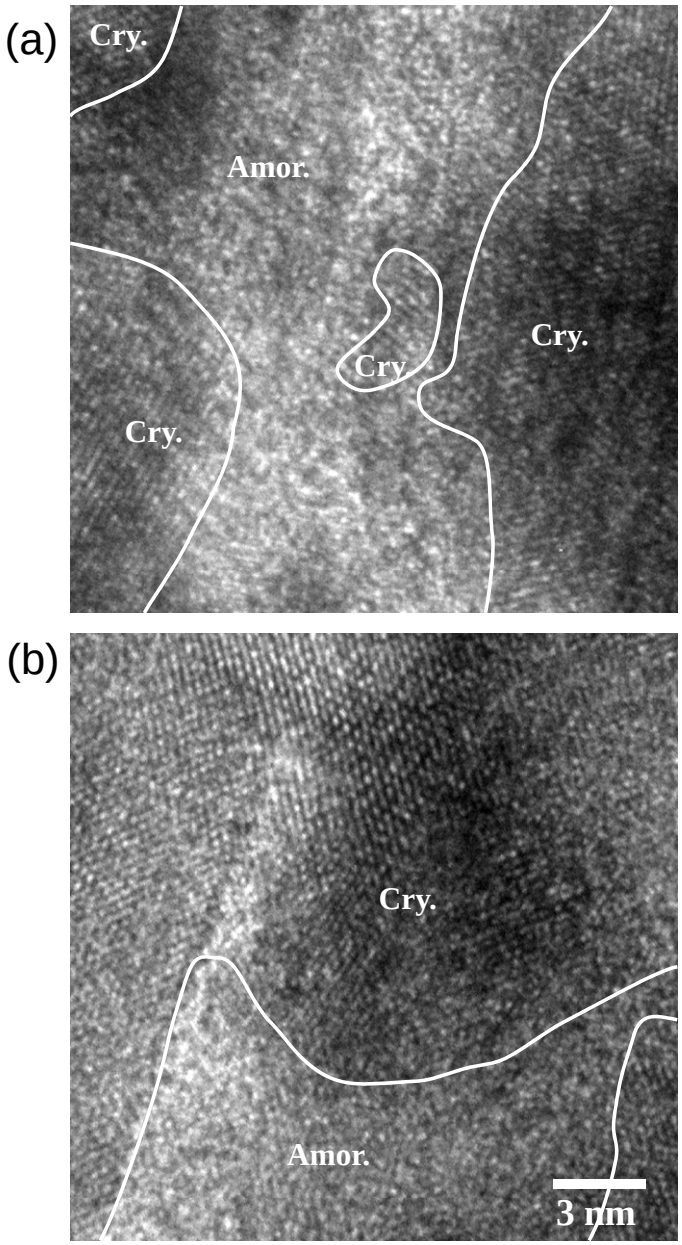

Figure 7. High-resolution transmission electron micrographs of ultramicrotomed vertical cross sections of the anodic oxide films formed on the sputter-deposited (a) Zr - 10 at% Si and (b) Zr - 11 at% Al alloys at 100 V in 0.1 mol dm^{-3} ammonium pentaborate electrolyte at 298 K for 900 s.

The mechanism of the capacitance enhancement of anodic ZrO_2 due to incorporation of silicon and aluminum species is illustrated in Figure 8. The formation of a composite oxide layer with a uniformly dispersed nanocrystalline high ε_{ox} oxide phase and amorphous low α oxide matrix phase was

responsible for the capacitance enhancement.

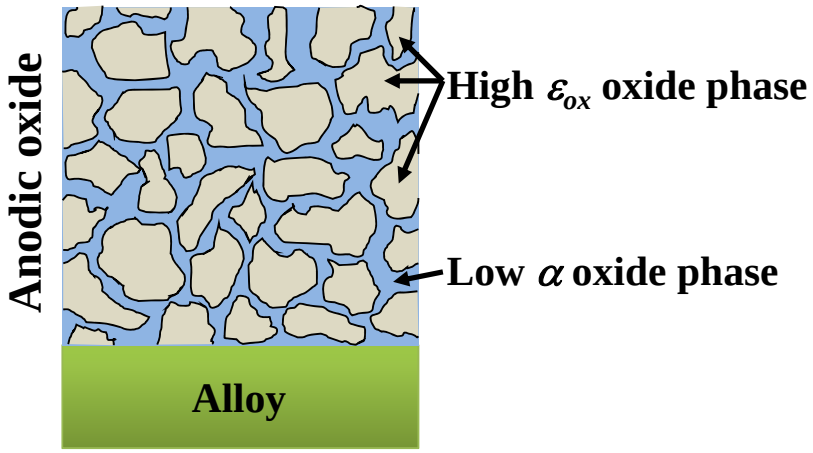

Figure 8. Schematic illustrations of the anodic oxide film consisting of high-ε_{ox} oxide nanocrystals and low-α amorphous oxide matrix.

4. CONCLUSIONS

This study demonstrated a new dielectric material design for capacitor application. By forming a composite anodic oxide layer comprised a nanocrystalline high-ε_{ox} oxide and highly resistive amorphous matrix, marked capacitance enhancement was achieved. For single-phase dielectric oxides formed by an anodizing process, there is a general empirical trend that oxides with higher permittivity form thicker films at a certain formation voltage. Thus, the capacitance enhancement is limited when a single-phase oxide is formed by adding elements that form high permittivity oxides. Utilization of a two-phase nanocomposite, with each phase having different roles in capacitance, eliminated this limitation. Examples of nanocomposite anodic ZrO_2–SiO_2 and ZrO_2–Al_2O_3 films were demonstrated in this study. The anodic oxide films contained nanocrystalline tetragonal ZrO_2 phase, which has higher permittivity than the monoclinic ZrO_2 that forms on zirconium metal. The phase separation of the tetragonal ZrO_2 produced silicon- or aluminum-enriched amorphous oxide matrix that could sustain a high electric field. Therefore, a thinner anodic oxide film with higher permittivity was developed, which

led to the high capacitance enhancement.

ACKNOWLEDGMENT

The present work was supported in part by the Global COE Program (Project No. B01: Catalysis as the Basis for Innovation in Materials Science) from the Ministry of Education, Culture, Sports, Science and Technology, Japan. The authors thank Mr. Tatsuto Nakamura of Horiba Ltd. for measuring the Raman spectra.

Supporting Information Available

Figures of the capacitance of anodic oxide films on Zr–Y alloys with various compositions and the characterization of anodic oxide films by Raman spectroscopy and GDOES. This material is available free of charge via the Internet at http://pubs.acs.org/.

REFERENCES

1. Takada, D.; Ishijima, M.; Murayama, Y., *NEC Tech J.* **2006,** *1*, 63-67.
2. Lopez-Lopez, G.; Lopez-Lopez, J.; Garcia-Yagues, M. R., *Dyna* **2009,** *84*, 219-224.
3. Robertson, J., *Eur. Phys. J.-Appl. Phys* **2004,** *28*, 265-291.
4. Watanabe, K.; Sakairi, M.; Takahashi, H.; Takahiro, K.; Nagata, S.; Hirai, S., *Elechem.* **2001,** *69*, 407-413.
5. Izumi, T., *Denkai Chikudenki Hyoron* **2010,** *61*, 94-98.
6. Harrop, P. J.; Campbell, D. S., *Thin Solid Films* **1968,** *2*, 273-292.
7. Habazaki, H.; Skeldon, P.; Shimizu, K.; Thompson, G. E.; Wood, G. C., *J. Phys. D: Appl. Phys.* **1995,** *28*, 2612-2618.
8. Habazaki, H.; Skeldon, P.; Shimizu, K.; Thompson, G. E.; Wood, G. C., *Corros. Sci.* **1995,** *37*, 1497-1509.
9. Habazaki, H.; Skeldon, P.; Thompson, G. E.; Wood, G. C.; Shimizu, K., *Philos Mag. B* **1995,** *71*, 81-90.

10. Habazaki, H.; Shimizu, K.; Skeldon, P.; Thompson, G. E.; Wood, G. C., *Thin Solid Films* **1997,** *300*, 131-137.

11. Habazaki, H.; Shimizu, K.; Skeldon, P.; Thompson, G. E.; Wood, G. C., *Proc. R. Soc. Lond. A* **1997,** *453*, 1593-1609.

12. Habazaki, H.; Shimizu, K.; Skeldon, P.; Thompson, G. E.; Wood, G. C.; Zhou, X., *Trans. Inst. Met. Finish.* **1997,** *75*, 18-23.

13. Habazaki, H.; Skeldon, P.; Thompson, G. E.; Wood, G. C.; Shimizu, K., *J. Mater. Res.* **1997,** *12*, 1885-1891.

14. Habazaki, H.; Matsuo, T.; Konno, H.; Shimizu, K.; Nagata, S.; Matsumoto, K.; Takayama, K.; Oda, Y.; Skeldon, P.; Thompson, G. E., *Electrochim. Acta* **2003,** *48*, 3519-3526.

15. Habazaki, H.; Ogasawara, T.; Konno, H.; Shimizu, K.; Asami, K.; Saito, K.; Nagata, S.; Skeldon, P.; Thompson, G. E., *Electrochim. Acta* **2005,** *50*, 5334-5339.

16. Habazaki, H.; Ogasawara, T.; Konno, H.; Shimizu, K.; Nagata, S.; Asami, K.; Takayama, K.; Skeldon, P.; Thompson, G. E., *J. Electrochem. Soc.* **2006,** *153*, B173-B177.

17. Santamaria, M.; Di Quarto, F.; Skeldon, P.; Thompson, G. E., *J. Electrochem. Soc.* **2006,** *153*, B518-B526.

18. Fogazza, M.; Santamaria, M.; Di Quarto, F.; Garcia-Vergara, S. J.; Molchan, I.; Skeldon, P.; Thompson, G. E.; Habazaki, H., *Electrochim. Acta* **2009,** *54*, 1070-1075.

19. Habazaki, H.; Takahiro, K.; Yamaguchi, S.; Shimizu, K.; Skeldon, P.; Thompson, G. E.; Wood, G. C., *Phil. Mag. A* **1998,** *78*, 171-187.

20. Habazaki, H.; Uozumi, M.; Konno, H.; Nagata, S.; Shimizu, K., *Surf. Coat. Technol.* **2003,** *169*, 151-154.

21. Habazaki, H.; Uozumi, M.; Konno, H.; Shimizu, K.; Nagata, S.; Asami, K.; Matsumoto, K.; Takayama, K.; Oda, Y.; Skeldon, P.; Thompson, G. E., *Electrochim. Acta* **2003,** *48*, 3257-3266.

22. Habazaki, H.; Uozumi, M.; Konno, H.; Shimizu, K.; Skeldon, P.; Thompson, G. E., *Corros. Sci.*

2003, *45*, 2063-2073.

23. Habazaki, H.; Shimizu, K.; Nagata, S.; Asami, K.; Takayama, K.; Oda, Y.; Skeldon, P.; Thompson, G. E., *Thin Solid Films* **2005,** *479*, 144-151.
24. Habazaki, H.; Uozumi, M.; Konno, H.; Shimizu, K.; Nagata, S.; Takayama, K.; Oda, Y.; Skeldon, P.; Thompson, G. E., *J. Electrochem. Soc.* **2005,** *152*, B263-B270.
25. Santamaria, M.; Di Quarto, F.; Habazaki, H., *Corros. Sci.* **2008,** *50*, 2012-2020.
26. Luby, S., *Thin Solid Films* **1976,** *32*, 61-64.
27. Sasaki, K.; Umezawa, T., *Kitami Inst Technol Repository* **1979,** *10*, 203-211.
28. Labunov, V.; Sokol, V.; Vorobiova, A.; Bondarenko, V., *Electrochim. Acta* **1985,** *30*, 1079-1084.
29. Koyama, S.; Aoki, Y.; Nagata, S.; Kimura, H.; Habazaki, H., *Electrochim. Acta* **2010,** *55*, 3144-3151.
30. Koyama, S.; Aoki, Y.; Sakaguchi, N.; Nagata, S.; Habazaki, H., *J. Electrochem. Soc.* **2010,** *157*, C444-C451.
31. Pringle, J. P. S., *Electrochim. Acta* **1980,** *25*, 1423-1437.
32. Chen, Y.; Sellar, J. R., *Solid State Ionics* **1996,** *86-8*, 207-211.
33. Lanagan, M. T.; Yamamoto, J. K.; Bhalla, A.; Sankar, S. G., *Mater. Lett.* **1989,** *7*, 437-440.
34. Zhao, X. Y.; Vanderbilt, D., *Phys. Rev. B* **2002,** *65*, 075105.
35. del Monte, F.; Larsen, W.; Mackenzie, J. D., *J. Am. Ceram. Soc.* **2000,** *83*, 1506-1512.
36. del Monte, F.; Larsen, W.; Mackenzie, J. D., *J. Am. Ceram. Soc.* **2000,** *83*, 628-634.
37. Murase, Y.; Kato, E.; Daimon, K., *J. Am. Ceram. Soc.* **1986,** *69*, 83-87.
38. Ishida, K.; Hirota, K.; Yamaguchi, O.; Kume, H.; Inamura, S.; Miyamoto, H., *J. Am. Ceram. Soc.* **1994,** *77*, 1391-1395.
39. Jerebtsov, D. A.; Mikhailov, G. G.; Sverdina, S. V., *Ceram. Int.* **2000,** *26*, 821-823.
40. Dörner, P.; Gauckler, L. J.; Krieg, H.; Lukas, H. L.; Petzow, G.; Weiss, J., *Calphad* **1979,** *3*, 241-257.

41. Koyama, S.; Y.Aoki; Nagata, S.; Habazaki, H., *J. Solid State Electrochemistry* **2011,** in press.

TOC graphic

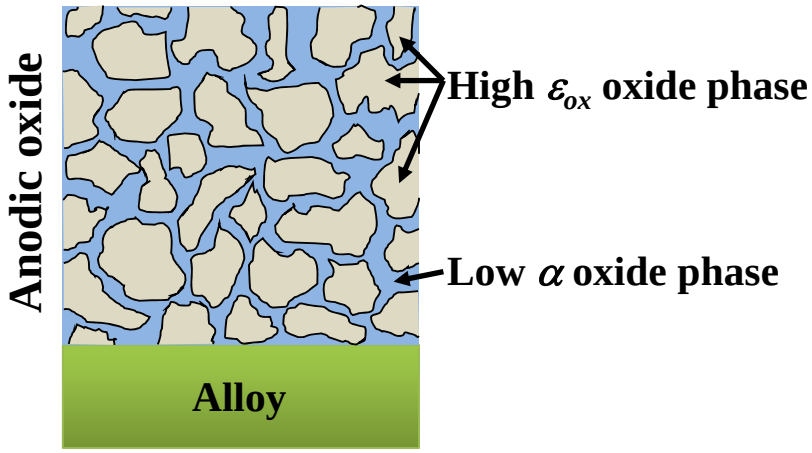
Anodic oxide
High ε_{ox} oxide phase
Low α oxide phase
Alloy